International Symposium
On Turbulence and Shear Flow
Phenomena (TSFP-9)
June 30 - July 3, 2015 *Melbourne, Australia*

NUMERICAL SIMULATIONS OF TURBULENT FLOW IN AN ECCENTRIC ANNULUS OF UNIT ECCENTRICITY

Nicolas Kanaris, Xavier Albets-Chico and Stavros Kassinos
Computational Sciences Laboratory (UCY-CompSci)
Department of Mechanical and Manufacturing Engineering
University of Cyprus, University Avenue 1, 2109 Nicosia, Cyprus
kassinos@ucy.ac.cy

ABSRACT

In this study, we perform Direct Numerical Simulations (DNS) of fully developed turbulent flows in eccentric annuli having different diameter ratios. Annuli of unit eccentricity, and diameter ratios of 0.2591 and 0.1395 have been investigated, for a Reynolds number of 14 600 based on the bulk velocity and outer wall diameter. This study aims to investigate the different flow characteristics, including the effect of the diameter ratio on the pressure gradient and the friction factor. Furthermore, this work confirms the presence of mean secondary flow for the configurations considered, while its effect on the flow characteristics and vortex structures is discussed in relation to the diameter ratios investigated.

INTRODUCTION

The relatively recent commercial implementation of concentrating solar power (CSP) plants with thermal energy storage (TES) has become a viable option for the dispatch of large-scale power generation plants based on renewable energy sources. Nowadays, most of the commercial TES systems use molten salts as a storage medium and also as the heat transfer fluid. Molten salts offer favorable storage capacities and perform well, from a technical point of view, at a relatively low cost. However, due to their relatively high melting point (eutectic solar salt 60% $NaNO_3$ - 40% KNO_3 melts around 230^o C) they pose a substantial thread to engineering systems employing them, since operating temperatures for the piping system are required to be maintained at high values (typically 265^o C) and freeze protection measures are needed. Slight deviations in electric heat tracing or thermal insulation performance, electrical blackouts or control failures can cause critical and catastrophic freezing events, leading to long shut downs and large replacement costs. Heat tracing applications typically install heat tracing cables on the outer surface of the pipelines, underneath a generally thick thermal insulation layer (Stehling & Alanis, 2012). Such *indirect* heat tracing systems are a robust solution, although not optimal for recovery from salt plug scenarios, as one is forced to heat up both the stainless steel pipeline and the related thermal insulation (despite their very high thermal inertia) before the melting process starts. A plausible alternative is to heat up the salts *directly* by installing heating cables inside the pipelines, therefore reducing the recover time and energy required to reopen hydraulic circuits inside the pipelines after freezing events. A potential drawback of this system, beyond the complexity associated with installation and maintenance, is its impact on the hydraulic operating parameters of the pipeline network. In particular, an increase in the pressure drop and friction factor characteristics due to presence of the heating cable is to be expected. Taking into account that the energy required for pumping is among the higher parasitic electrical consumptions of a CSP power plant, quantifying the potential pressure drop increase is fundamental to demonstrating the viability of this alternative approach.

This kind of *direct* heat tracing systems can be represented by annular duct flows with unit eccentricity, i.e. with the inner and outer surfaces of the annulus in direct contact. A number of experiments and numerical simulations on turbulent, concentric and eccentric annular duct flows have been performed in the past (Jonsson & Sparrow, 1966; Bourne *et al.*, 1968; Nouri *et al.*, 1993; Chung *et al.*, 2002; Nikitin *et al.*, 2009; Merzari & Ninokata, 2009). On the other hand, turbulent flow in an eccentric annulus with unit eccentricity has received much less attention because of the numerical difficulties in precisely treating such complex curved geometries. To our knowledge only a few experimental studies have been performed by Jonsson & Sparrow (1966), Nouri *et al.* (1993) and Bourne *et al.* (1968), with the latest having been contacted a few decades ago. In their studies they have shown that the diameter ratio (i.e. the ratio of the inner surface diameter to the outer surface diameter) is an important parameter with respect to friction factor characteristics. Interestingly, at high eccentricities (0.9 and 1) and low diameter ratios (0.281), Jonsson & Sparrow (1966) reported difficulties in determining the local shear distribution on the inner wall, which they attributed to the presence of secondary flow. These studies, however, were limited to diameter ratios ranging from 0.25 to 0.95, while in heat tracing applications smaller diameter ratios ranging from 0.3 to 0.02, and even lower, are of practical interest.

The present work aims to fill in the gap in the area of low diameter ratios for the case of turbulent flow through an annulus of unit eccentricity. The focus is on investigating in detail the flow characteristics and frictional pressure drop characteristics. This is a key feature when considering the viability and engineering optimization of such heat tracing applications in solar fields. During normal operation of such a system, Reynolds numbers in the range $14\,600 \leq Re \leq 146\,000$ (based on the bulk velocity and outer wall diameter) are expected. In this work, results will be presented only for the lower extremum value of $Re = 14\,600$ utilizing Direct

Table 1. Geometrical and numerical parameters for the different cases investigated.

Case	α	e	L/D	Total nodes
C1	0	1	5	19 003 482
C2	0.1395	1	5	12 970 389
C3	0.2591	1	5	12 109 671

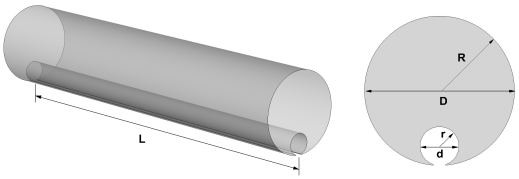

Figure 1. Schematic represantation of flow configuration.

Numerical Simulations.

PROBLEM FORMULATION

We consider the flow through an eccentric circular annulus, as shown in Figure 1. The geometry consists of a small cylindrical surface of diameter, d, encased and in direct contact with a cylindrical surface of larger diameter, D, and length L. The ratio of the inner wall diameter to the diameter of the outer wall, defines the diameter ratio, α, while the distance between the centres of the inner and outer cylinders, s, is associated with the eccentricity, e, as:

$$\alpha = \frac{d}{D}, \quad e = \frac{s}{D-d} \tag{1}$$

A geometry with unit eccentricity (walls in contact) has been chosen, since this configuration corresponds to a heating cable (inner wall) resting at the bottom of a solar field pipeline (outer wall). In order to identify the influence of the inner wall (heating cable) diameter on the computed flow characteristics, two specific diameter ratios were considered, $\alpha = 0.2591$ and $\alpha = 0.1395$. In addition, the case of a plain circular pipe in the absence of a smaller inner surface has been considered, i.e. $\alpha = 0$, for validation purposes and to serve as a reference point. The length of the computational domain was set to $L = 5D$, which is considered sufficient for the development of all large turbulent structures at this Reynolds number (Eggels *et al.*, 1994). The dimensions of the different flow configurations investigated are summarized in Table 1.

The flow of an incompressible, Newtonian fluid is described by the set of Navier-Stokes equations. Using the diameter of the outer pipe, D, and the bulk flow velocity, U_b, as the characteristic length and velocity scales respectively, the non-dimensional continuity and momentum equations in a Cartesian coordinate system are given by

$$\frac{\partial u_i}{\partial x_i} = 0 \tag{2}$$

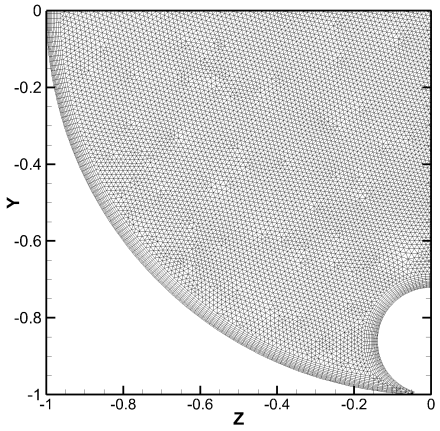

Figure 2. Close-up, cross-section of grid for case C3.

Table 2. Variation of the pressure gradient along the pipe for different diameter ratios.

Case	$\Delta P/L$	Rell. Diff. $\Delta P/L$
C1	7.00×10^{-3}	–
C2	7.90×10^{-3}	10%
C3	9.01×10^{-3}	26%

$$\frac{\partial u_i}{\partial t} + \frac{\partial u_i u_j}{\partial x_j} = -\frac{\partial p}{\partial x_i} + \frac{1}{Re}\frac{\partial^2 u_i}{\partial x_j \partial x_i} \tag{3}$$

where $Re = U_b D/\nu$ is the Reynolds number. Here, ν is the kinematic viscosity of the fluid.

The above equations are solved using the unstructured nodal-based finite-volume code CharLES, developed at the Center of Turbulence Research (Stanford/NASA Ames), as a general platform, and imposing periodic boundary conditions for the velocity component in the streamwise direction. Details of the code have been described extensively in Ham *et al.* (2006), and Moin & Apte (2006). Numerical simulations have been performed on different non-uniform grids, consisting of quadrilateral elements in the boundary layer and triangular elements in the center region (see Figure 2). Grid resolution was varied in each case, so as the distance from the duct walls to the first node was $\Delta y^+_{1st} \approx 1$, the maximum spacing in the direction normal to the wall $\Delta r^+_{max} \approx 5$, and the maximum streamwise spacing $\Delta z^+ \approx 7$, in terms of wall units. The total number of nodes of the various grids used can be seen in Table 1.

RESULTS

All simulations are initiated from randomly generated flow fields and advanced in time until computations reached a statistically steady state. Figure 3 shows snapshots of the streamwise velocity field, u_x, in planes $z = 0$ and $x = L/2$, for a fully developed flow corresponding to all cases investigated (see Table 1).

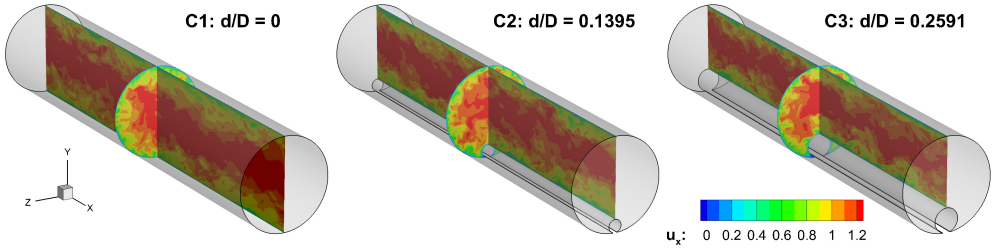

Figure 3. Contour plots of streamwise velocity, u_x, in planes $z = 0$ and $x = L/2$ for all cases at $Re = 14\,600$.

Pressure field

Table 2 shows the pressure gradient along the pipe, as a function of the diameter ratio, where $\Delta P/L$ is defined as the mean pressure gradient between the inlet ($x = 0$) and the outlet ($x = L$) boundary. In order to highlight the magnitude of the pressure drop in the cases when an inner wall is present (cases C2, C3), the relative differences with respect to a plain pipe (case C1), are also shown. As shown here, for a fixed value of Re and with increasing diameter ratio, the pressure drop gradient increases, as expected. For the higher diameter ratio, 0.2591, this pressure drop is quite significant when compared to a plain pipe, approximately 26%. However for the smaller diameter ratio, 0.1395, the pressure drop is reduced to 10%. From an engineering point of view, this initial analysis shows that for specific combination of heating cables and pipeline diameters, the increased pressure drop (and related costs) of this new heat tracing alternative is relatively small and, henceforth, viable.

In smooth pipes, the non-dimensional pressure drop is also usually presented in terms of the Darcy friction factor,

$$C_f = \frac{(\Delta P/L)\, D_h}{\frac{1}{2}\rho U_b^2} \tag{4}$$

Here, D_h is the hydraulic diameter, which depends on the channels cross-sectional geometry, and is equal to $R - r$. Figure 4 shows the variation of the Darcy friction factor as a function of the Reynolds number, for the different diameter ratios considered. Results from the present numerical simulations are compared against previous experimental studies in annular ducts of unit eccentricity, although for different aspect ratios. In those studies, results have been correlated by power law relationships of the type $C_f = C/Re^n$, with each study yielding different coefficients and exponents over the various configurations and range of Reynolds number investigated. These correlations are shown in this figure using dashed lines. The solid line indicates the Blasius approximation for a turbulent pipe flow. As shown here, there are large discrepancies between the experimental studies, ranging from 10% up to 25%. Nevertheless there is a fairly good qualitative agreement with respect to the variation of the friction factor, which decreases with increasing Reynolds. For a given Re the friction factor also increases as the diameter ratio is increased. This is line with current observations. In addition, for $\alpha = 0$ the agreement between current results and the Blasius approximation is very good. On the other hand, for $\alpha = 0.2591$ the percentage difference between current data with respect to the ones obtained by Bourne *et al.* (1968) is around 10%. The results of Bourne, however, correspond to slightly larger diameter ratio and this might explain part of the discrepancy.

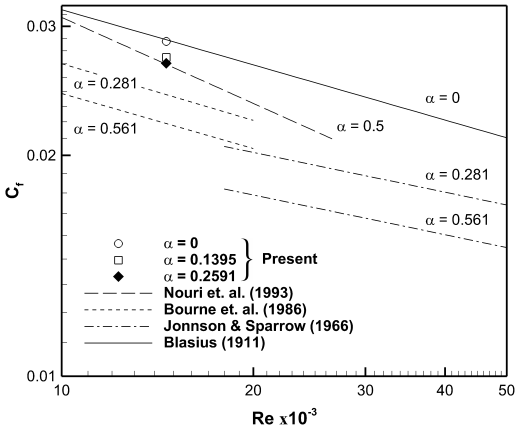

Figure 4. Darcy friction factor, C_f, as a function of Reynolds number, Re, for different diameter ratios, α. Current results (symbols) are compared against previous experimental studies in annular ducts of unit eccentricity (dashed lines), and the Blasius approximation for a turbulent pipe flow (solid line).

Secondary mean motion

The mean streamwise velocity field at a cross-section of the flow is shown in Figure 5, for all diameter ratios investigated. Contour lines of the mean velocity in the y-direction, are superimposed in Figures 5(a-c). The juxtaposition of the mean velocity components, parallel ($U_{x,\,avg}$) and normal ($U_{y,\,avg}$) to the flow, indicates the presence of secondary motion perpendicular to the streamwise flow direction in the cases of low diameter ratios (see Figs. 5b and 5c). The maximum velocity in the cross-flow direction is 3.7% and 2.4% of the maximum mean streamwise velocity for diameter ratios $\alpha = 0.1395$ and $\alpha = 0.2591$, respectively. The later value, is similar with the results of Nouri *et al.* (1993) who measured values of the secondary flow up to 2.5% of the bulk flow, for a configuration with the same eccentricity but a larger (almost double) diameter ratio, $\alpha = 0.5$. Interestingly, it appears that the diameter ratio in the range 0.25 to 0.5 has little effect on the magnitude of the secondary motion, while at smaller values one can observe an almost 50% increase. Such secondary mean-flow patterns in the cross-section of an eccentric annulus are an intrinsic feature of the flow. This cross-stream transfer of momentum could be of practical importance in the heat tracing of molten salt pipes, where enhancement of mixing and heat transfer from the heated cable to the molten salt is desired.

The distribution of the mean streamwise velocity as a

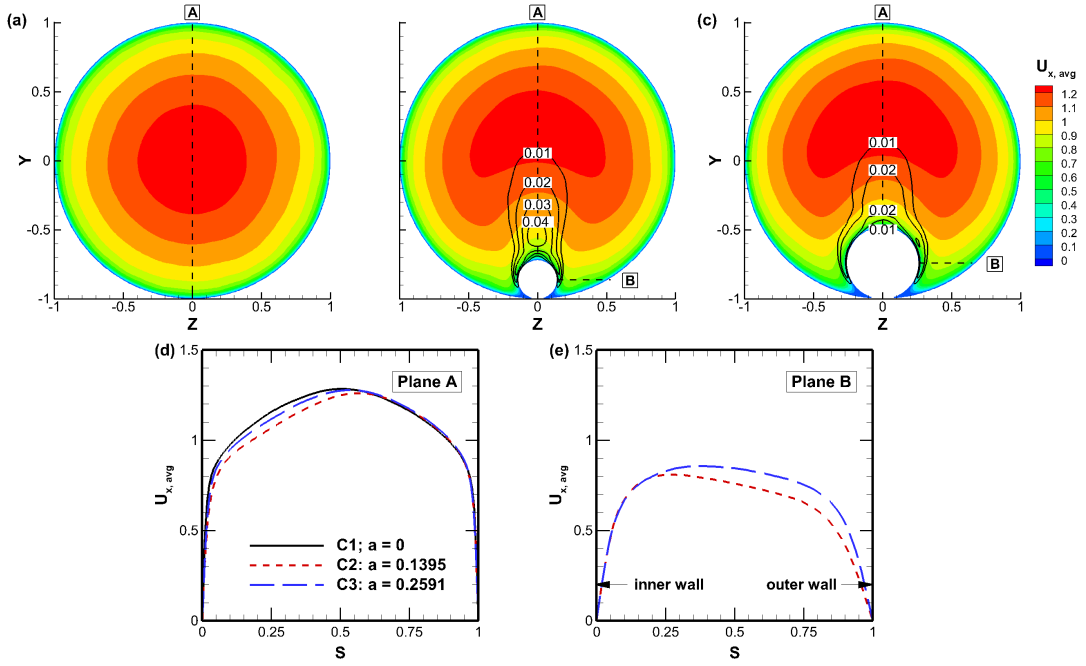

Figure 5. Visualization of the mean stremwise velocity field, $U_{x,\,avg}$. (a-c) Contour plots of $U_{x,\,avg}$ in the plane $x = 5$. Solid lines correspond to contour lines of mean velocity in the y-direction, $U_{y,\,avg}$. (d-e) Distribution of $U_{x,\,avg}$ as a function of the normalized distance from the inner to the outer wall, S, in the planes $x = 5$, $z = 0$ (plane A) and $x = 5$, $y = R - r$ (plane B).

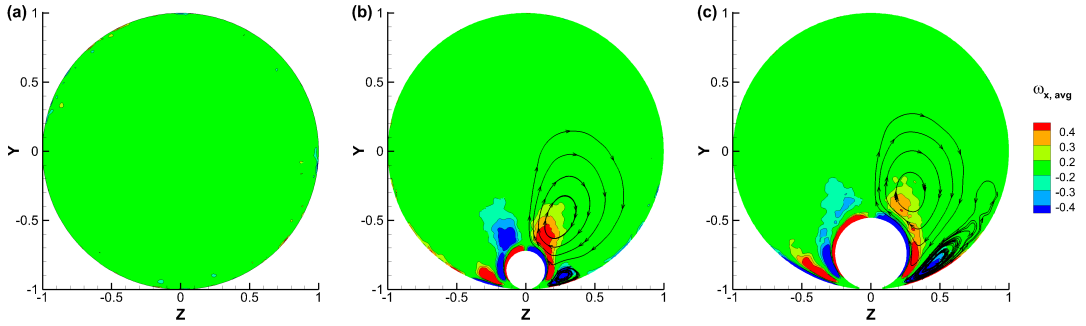

Figure 6. Visualization of the mean streamwise vorticity component. Streamlines are constructed from the in-plane mean velocity field. For the sake of clarity, streamlines are only shown on the right-half symmetry plane.

function of the normalized distance from the inner to the outer wall, in the planes $z = 0$ (plane A) and $y = R - r$ (plane B), is shown in Figures 5(d-e). In case C1 ($\alpha = 0$) one can observe the typical average velocity profile for turbulent flow in a pipe, with a large, relatively flat core, and sharp velocity gradients near the pipe walls. For cases C2 ($\alpha = 0.1395$) and C3 ($\alpha = 0.2591$), the velocity profiles are skewed with the point of maximum velocity being closer to the outer wall in both cases. As the diameter ratio is increased the velocity profile becomes less inclined. This in line with the experimental observations of Nouri *et al.* (1993) who observed even less inclined velocity profiles, for an even larger diameter ratio, $\alpha = 0.5$.

The effect of the secondary motion on the mean flow, is depicted on the averaged streamwise vorticity component, and the associated streamlines constructed from the mean velocity field, as illustrated in Figure 6. For the sake of clarity, streamlines are only shown on the right-half symmetry plane. As expected, in the case of a straight pipe (case C1) due to the one-directional character of the mean flow, no streamwise vorticity is observed. On the other hand, in the cases of annular flow (cases C2, C3) the secondary motion yields streamwise vortex pairs at the vicinity of the inner wall. Two pairs of recirculating flow are evident in the flow, with the larger pair positioned on top of the inner wall, and the smaller one squeezed in between the inner and outer wall. Similar flow patterns have also been obtained for a larger diameter ratio, $\alpha = 0.5$, in the experimental work of Nouri *et al.* (1993) for the same eccentricity and the numerical investigations of Merzari & Ninokata (2009) for $e = 0.8$. As the diameter ratio is decreased, the larger vortex pair become even more dominant in the flow, displacing the smaller recirculating regions closer to the outer wall. This is related with the stronger secondary velocity for $\alpha = 0.1395$, and may explain the inclined velocity profiles mentioned before.

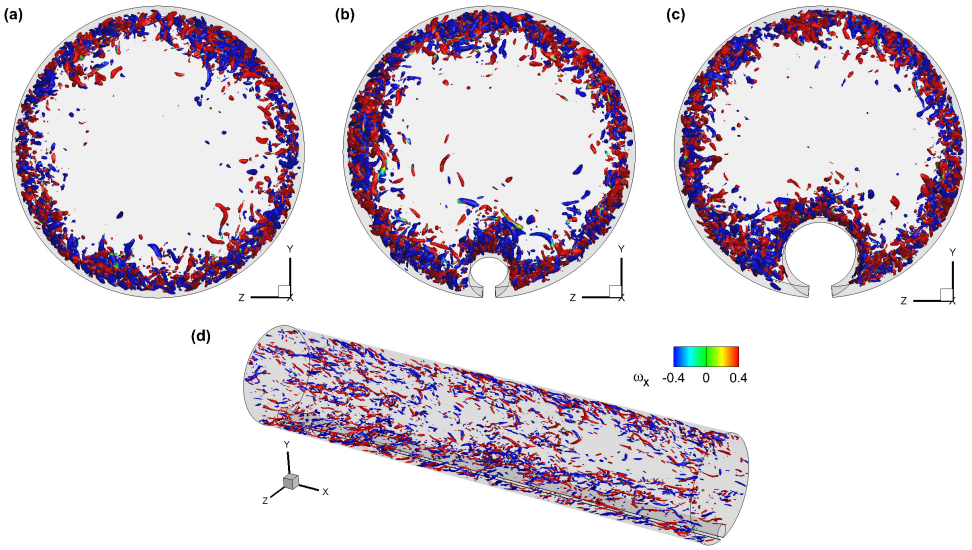

Figure 7. Iso-surfaces of the λ_2 criterion normalized by its absolute minimum ($\lambda_2/\lambda_{2,\,min} = 10\%$) at instantaneous time. Iso-surfaces are colored by the spanwise vorticity component.

Three-dimesniponal Instabilities

An effective way of visualizing the vortex structures in a turbulent pipe flow, is through the application of the λ_2 criterion proposed by Jeong & Hussain (1995). λ_2 is defined as the second eigenvalue of $S^2 + X^2$, where S and X denote the symmetric and antisymmetric parts of the velocity gradient tensor, respectively. Using iso-surfaces of the λ_2 criterion, one can identify three-dimensional vortical motions in the flow, while excluding the near-wall shear region. Figure 7 presents snapshots of iso-surfaces of λ_2 for all cases. In order to reveal the streamwise rotation direction of each vortical structure, iso-surfaces are colored by the streamwise vorticity component, $\omega_{x,\,avg}$. In all cases, longitudinal, tubular vortices can be observed, which are confined in the region close to the inner and outer wall of the duct. Similar patterns have been observed in annular ducts before by Merzari & Ninokata (2009) and Motlagh *et al.* (2013), although for different geometrical parameters. In case C2, there seems to be a tendency for stronger accumulation of vortices in the vicinity on top of the inner cylinder. This effect is probably correlated with the stronger secondary mean-motion at this diameter ratio when compared with case C3. Further work is needed to better understand the contribution of these near-wall vortical structures to turbulence production and the extent to which they affect heat transfer characteristics.

CONCLUSIONS

Direct numerical simulations of the three-dimensional turbulent flow in an annular duct of unit eccentricity, $e = 1$, have been performed.Three diameter ratios have been investigated, namely $\alpha = 0$ (plain circular pipe), $\alpha = 0.1395$ and $\alpha = 0.2591$, while the Reynolds number was kept constant at $Re = 14600$. The effect of the diameter ratio on the pressure drop and friction factor has been shown. Also, present results confirmed the presence of secondary mean motion, at small diameter ratios, and its effect on the flow characteristics and vortex structures has been demonstrated.

REFERENCES

Bourne, D. E., Figueiredo, O. & Charles, M. E. 1968 Laminar and turbulent flow in annuli of unit eccentricity. *Can. J. Chem. Eng.* **46**, 289–293.

Chung, S. Y., Rhee, G. H. & Sung, H. J. 2002 Direct numerical simulation of turbulent concentric annular pipe flow Part 1: Flow field. *Int. J. Heat Fluid Flow* **23**, 426–440.

Eggels, J. G. M., Unger, F., Weiss, M. H., Westerweel, J., Adrian, R. J., Friedrich, R. & Nieuwstadt, F. T. M. 1994 Fully developed turbulent pipe flow: A comparison between direct numerical simulation and experiment. *J. Fluid Mech.* **268**, 175209.

Ham, F., Mattson, K. & Iaccarino, G. 2006 Accurate and stable finite volume operators for unstructured flow solvers. Annual Research Briefs, Center for Turbulence Research. Stanford University/NASA Ames.

Jeong, J. & Hussain, F. 1995 On the identification of a vortex. *J. Fluid Mech.* **285**, 69–94.

Jonsson, V. R. & Sparrow, E. H . 1966 Experiments on turbulent-flow phenomena in eccentric annular ducts. *J. Fluid Mech.* **25**, 65–86.

Merzari, E. & Ninokata, H. 2009 Anisotropic turbulence and coherent structures in eccentric annular channels. *Flow Turbulence Combust* **82**, 93–120.

Moin, P. & Apte, S. V. 2006 Large-eddy simulation of realistic gas turbine combustors. *AIAA Journal* **44**, 698–708.

Motlagh, Y.G., Ahn, H.T., Hughes, T.J.R. & Calo, V.M. 2013 Simulation of laminar and turbulent concentric pipe flows with the isogeometric variational multiscale method. *Computers & Fluids* **71**, 146–155.

Nikitin, N., Wang, H. & Chernyshenko, S. 2009 Turbulent flow and heat transfer in eccentric annulus. *J. Fluid Mech.* **638**, 95–116.

Nouri, J. M., Umur, H. & Whitelaw, J. H. 1993 Flow of Newtonian and non-Newtonian fluids in concentric and eccentric annuli. *J. Fluid Mech.* **253**, 617–641.

Stehling, L. & Alanis, J. 2012 Electric heat tracing controls: its integration in industrial facilities. *IEEE Industry Applications Magazine* **18**, 60–69.